Supplementary Information for "Realization of quasi-1D topological magnetism at the V alloyed MoS_2 zigzag edge"

Kejie Bao[1], *Junyi Zhu*[1,*]

[1]Department of Physics, The Chinese University of Hong Kong, Shatin, Hong Kong SAR, China

[*]Email: jyzhu@phy.cuhk.edu.hk

The SM provides detailed illustrations on topological transition in the trimer SSH model, details and convergence tests for DFT calculations, explanations on the electron counting model, stability of the V chain, the effects of SOC and Hubbard U, method to compute the parameters for trimer SSH, and Wannier functions for intrinsic edge and spin-up channel of V-alloyed edge.

1. Mermin-Wagner theorem.

In this section, we briefly illustrate the Mermin-Wagner theorem in the 1D system by taking isotropic Heisenberg model as an example[1,2]. The quantum Heisenberg model with an external magnetic field B_0 can be expressed as ($\hbar$ and μ_B are assumed to be 1 here):

$$\hat{H} = \sum_{i,j} J_{ij} \hat{S}_i \cdot \hat{S}_i + \sum_i B_0 S_i^z e^{ik \cdot R_i}, \#(3)$$

where the exchange integral J_{ij} decays sufficiently fast with increasing distance $|R_i - R_j|$ so that the quantity $Q = \frac{1}{N}\sum_{ij} |J_{ij}| |R_i - R_j|$ remains finite. In finite temperature, the induced magnetization in thermodynamic limit is given as:

$$M(T) = lim_{B \to B_0} \frac{1}{N} \sum_i e^{ik \cdot R_i} \langle S_i^z \rangle. \#(4)$$

In 1D, we could explicitly evaluate the upper bound of $M(T)$ as:

$$|M(T)| \leq const. \frac{B_0^{\frac{1}{3}}}{T^{\frac{2}{3}}}, as\ B_0 \to 0. \#(5)$$

Therefore, there is no spontaneous magnetization in the 1D system because

$M(T) = 0$ for $B_0 = 0$ at finite temperature T. However, the Mermin-Wagner theorem is only valid for the isotropic case and even weak anisotropy could lead to the emergence of magnetic order. Therefore, in our quasi-1D system, because of the structural anisotropy, it is possible to stabilize the magnetic ordering at the edge. Furthermore, the spin-orbit coupling of the V atom or Mo atom could also provide extra anisotropy and help to stabilize the long-range order along the edge[2].

2. Topological transition in trimer SSH model

In this section, we briefly summarized the topological transition of the 1D-chain based on trimer SSH model[3]. We mainly focus on the inversion symmetry preserved case, specifically, $u = v$ and $\mu_A = \mu_C$. As the increment of the inter-cell hopping integral *w*, the end states emerge with the Zak phase changing from 0 to 1, as shown in SI Fig.1. When the inversion symmetry is broken with $u \neq v$, the end state also can be realized, however, the two end states are not equal. Specially, when $u < w < v$ or $v < w < u$, there is only one end state localized at either left or right end. Based on our Wannier function analysis, the intra-cell hopping integrals for the V-alloyed edge are very close and smaller than the inter-cell hopping, therefore, we can still observe two end states.

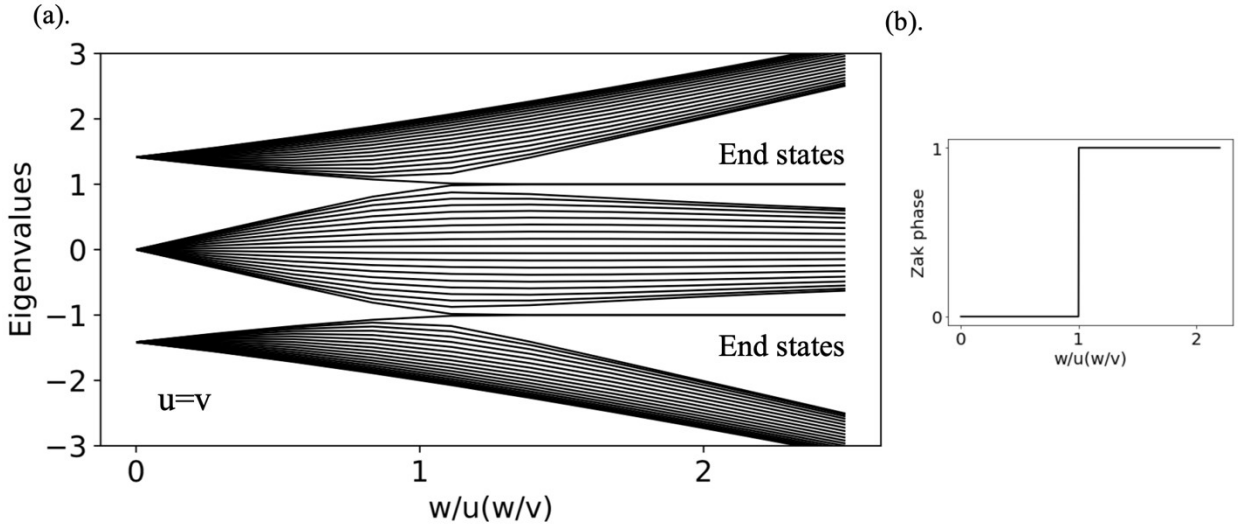

SI Figure 1. (a) Evolution of the end states and (b) the Zak phase as the increment of the intercell hopping w. The figure is adapted from reference[3]. Reproduced with permission from Phys. Rev. A 99, 013833. Copyright 2019 American Physical Society.

3. Electron counting model (ECM) in MoS_2 systems and passivation of the bottom edge

We summarized the ECM in MoS_2 based on literature[4] in this section. ECM in MoS_2 systems is determined by the charge allocation in S-Mo bonds. Basically, three types of charge distributions exist following different assumptions on the local symmetry and electron filling for S and Mo atoms. The counting details are elaborated on below:

(a) 1.33e and 0.67e per S-Mo pair[5]. The model first considers the electron distribution in Mo atoms with the assumption that the local symmetry of Mo atoms is 6-fold. Since Mo atom has a chemical valence of $+4$ in MoS_2, each Mo atom donates 4 electrons equally to 6 neighboring S atoms, leading to $4 \div 6 = 0.67$ electrons per Mo-S bond. For S atom, two electrons occupy the lone pair state along z direction of the S and the remaining 4 valence electrons distribute equally to 3 nearby S atoms, leading to $4 \div 3 = 1.33$ electrons per Mo-S bond. Therefore, if two dangling bonds of the two S atoms at the edge form dimers, $1.33 \times 2 - 2 = 0.66$ electrons will be excessive. We mainly applied charge allocations of 1.33e and 0.67e per S-Mo pair to analyze the edge reconstructions at the S edge, inferred from the emergence of the reconstruction with $3\times$ periodicities.

(b) 1.5e and 0.5e per S-Mo pair[6]. We consider the S atoms first and propose that 6 valence electrons of S atoms are distributed equally into the 4 bonds, including 1 lone pair state and 3 Mo-S bonds, resulting in $6 \div 4 = 1.5$ electrons per bond. For Mo atom, 3 of 4 valence electrons are distributed equally to 6 neighboring S atoms, resulting in $3 \div 6 = 0.5$ electrons per Mo-S bond. The remaining 1 electron will transfer to the two partially occupied S lone pair states on the top and bottom surface equally.

(c) 1.66e and 0.33e per S-Mo pair[6]. For S atom, 5 electrons are distributed equally to 3 Mo-S bonds and each bond has $5 \div 3 = 1.67$ electrons. The remaining 1 electron is in the dangling bond. For Mo atoms, 2 of 4 electrons are distributed equally to 6 Mo-S bonds, resulting in $2 \div 6 = 0.33$ electrons per Mo-S bond. The remaining 2 electrons transfer to the two partially occupied S dangling bonds on the top and bottom surface.

In addition, the long-range dipole-dipole interaction and electron transfers between the top edge and bottom edge may significantly affect their edge reconstructions. More importantly, the interaction and electron transfers may induce large numerical errors in the calculations of zigzag edges, leading to discrepancies between experiments and calculations[7]. Also, reconstructions of bare edges may induce a large structure distortion, which can be long-range. To reduce the quantum coupling and mechanical interactions between the two edges and investigate the edge states localized at either edge, pseudo-Hs with fractional charge are proposed to passivate the polar zigzag edges, based on the ECM.

Because all the charge allocations satisfy ECM, as mentioned in the previous section, extra evidence is needed to determine the most stable passivation scheme. Recently, CK.Sin *et al* suggested that using 0.5 electrons and 1.5 electrons to passivate the S and Mo edges induces the smallest structure distortion and can mimic the atomic structure of the bulk reasonably well[6]. Therefore, in this work, we applied two pseudo-Hs with 1.5 electrons to passivate the two dangling bands of the Mo atoms at the bottom edge.

4. Details and convergence tests for DFT calculations

In this section, the calculation details and convergence tests are illustrated. For DFT calculations, the Energy cutoff of the plane wave to expand the wavefunction was up to 500eV and $(23 \times 1 \times 1)$, $(11 \times 1 \times 1)$, and (

$7 \times 1 \times 1$) k-points were used to sample the Brillouin zone of the $1\times$, $2\times$, and $3\times$ periodicities, respectively. Electronic relaxations were converged to 10^{-5} eV and ionic relaxations were converged until all atomic forces are less than 0.01 eV/Å. The convergence tests for the energy cut-off, k-points sampling, vacuum thickness, and width of the ribbon were carefully performed. The convergence tests for the energy cut-off, k-points sampling, vacuum thickness in y direction and z direction, and width of the ribbon were carefully performed in the V-related supercell with $1\times$ periodicity as an example, as shown in SI Fig. 2(a)~(e). For vacuum thickness in the y direction, the energy for 20Å is significantly lowered, probably because of the existence of the quantum coupling between two edges. Therefore, we chose 30Å in our calculations. In addition, for the convergence test about the ribbon width, the super-linear curve indicates that the change of the total energy remains constant when a certain amount of Mo and S atoms are included in the system, serving as evidence of the convergence.

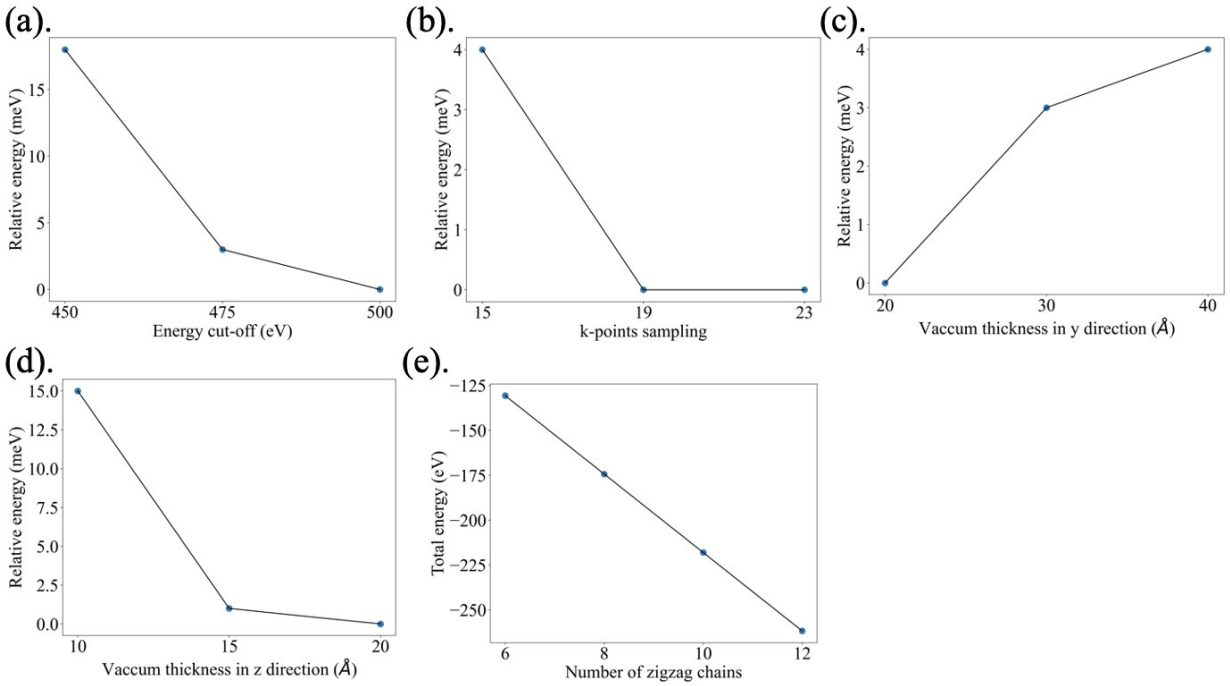

SI Figure 2. Convergence tests for (a) energy cut-off, (b) k-points sampling, (c) vacuum thickness in the y direction, (d) vacuum thickness in the z direction, and (e) thickness of the ribbon.

Moreover, the DFT+U method was clarified in this section. For systems with strong correlations, DFT usually fails in predicting the correct band gap[8,9]. One of the corrective approaches is to add Hubbard U corrections to the localized orbitals[8]. The idea of the U term is based on the Hubbard model[10]:

$$\hat{H} = \sum_{<i,j>,\sigma} t_{ij} c_{i,\sigma}^{\dagger} c_{j,\sigma} + U \sum_{i} n_{i,\uparrow} n_{i,\downarrow}, \#(1)$$

where t_{ij} is the hopping integral between nearest-neighboring atomic sites and U represents the onsite Coulomb repulsion, and other terms corresponding to the long-range Coulomb repulsion between different sites are

neglected. $n_{i,\uparrow}$, $c_{i,\sigma}^{\dagger}$, and $c_{i,\sigma}$ are electron density, electron creation, and annihilation operators. Based on the Hubbard model, the DFT+U scheme is established with the Hubbard U term added to the localized d or f orbitals. Especially, because of the localization of 3d orbitals for transition metal atoms, Hubbard U values are generally required for accurate predictions[11]. For example, U = 3eV was widely used to treat the localized d orbitals of V atoms in V-based sulfide systems, such as VS and VS_2[12]. DFT+U method could enhance the prediction of the physical properties with considerably lower computational cost[13].

To illustrate the influence of the Hubbard U, we further compared the band structures obtained from DFT method to those obtained from the DFT+U method shown in Fig. 2 in the manuscript. As shown in SI.Fig.3, If the Hubbard U term is not included, the spitting of the edge band in the spin-up channel and the spin-down channel is smaller due to the reduction of the exchange interaction. It will also result in the edge bands of the spin-up channel dominating near the Fermi level, rather than the spin-down channel when U = 3 eV is applied. The semiconducting nature is preserved, while the band edge shifts from the Γ valley to the X valley, as shown in SI.Fig.3. The gap of the spin-up channel is about 129 meV for the U = 0 case, which is comparable to the gap value of about 79 meV for the U = 3 eV case. The difference between the U = 0 and U = 3 eV cases indicates that the Coulomb interaction is crucial in determining the band structure of the edge bands.

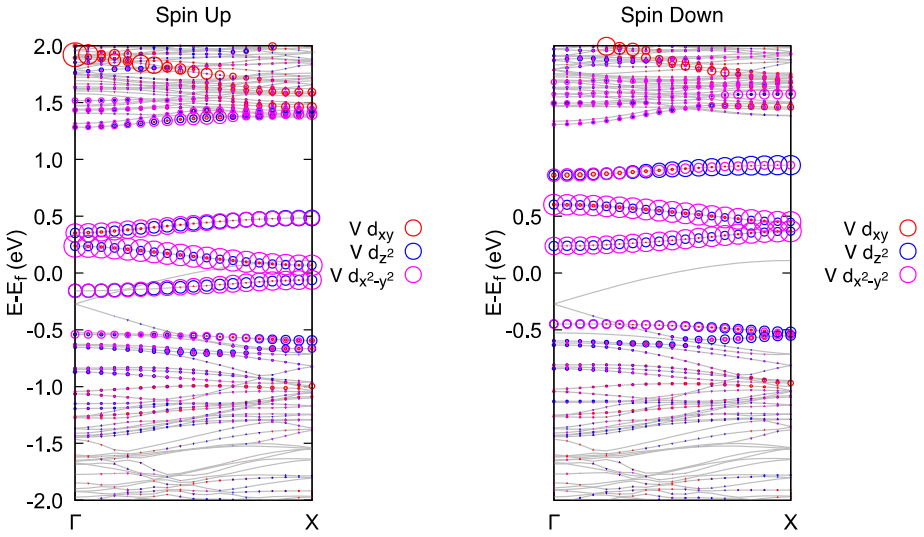

SI Figure 3. Band structures for V-alloyed S-oriented edge for 3 × periodicities when GGA method is applied. The symbols follow Fig. 2 in the manuscript.

---

5. Stability of the V chain

In this section, we first illustrated the stability of the interface between the V chain and the edge. We found that the formation energy of the V chain 3 × periodicities is decreased from the S-poor to the S-rich condition,

as shown in SI Fig.3. Remarkably, the formation energy is negative in the S-rich condition, indicating the stability of the V chain. Additionally, we also calculated the formation energy of two nearest-neighboring V atoms incorporated into the monolayer of MoS_2 as the reference. Specifically, two V atoms are introduced into (5×5) monolayer to ensure a similar concentration. To make a fair comparison with the nearby V atoms at the edge, the two V atoms replace the nearest-neighboring Mo sites in the monolayer. We found that the V atoms prefer to stay near the edge rather than in the bulk of the monolayer, as shown in SI Fig.4.

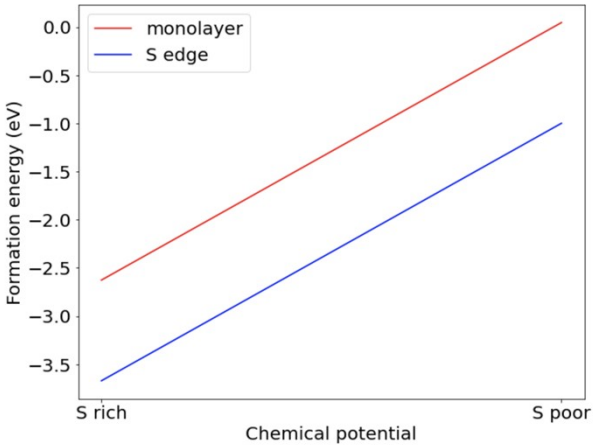

SI Figure 4. The formation energy of the V atoms alloyed S-oriented edges with 3 × periodicities. The formation energy of two nearest-neighboring V atoms in the bulk is taken as a comparison.

---

6. SCAN+ U method

In this section, method with a higher accurate exchange and correlation functional was applied to verify our findings. Because our system contains nearly 100 atoms and about 20Å vacuum along the x and y directions, the HSE calculation is time-consuming and beyond our computational capability. Instead, we try the strongly constrained and appropriately normed (SCAN) functional[14] to give more evidence of the gap-opening nature when 3 × periodicities are taken into consideration. It was believed that SCAN functional could give a more accurate prediction of the band gap because the evaluation of the exchange-correlation functional is improved[14]. As shown in SI. Fig. 5, the band structure obtained by SCAN+U method is similar to that obtained from DFT+U method. However, the SCAN+U method predicted a larger band gap at the Fermi level, about nearly 155 meV. This is because the band gap is usually underestimated by GGA functional, while SCAN could provide a more accurate prediction.

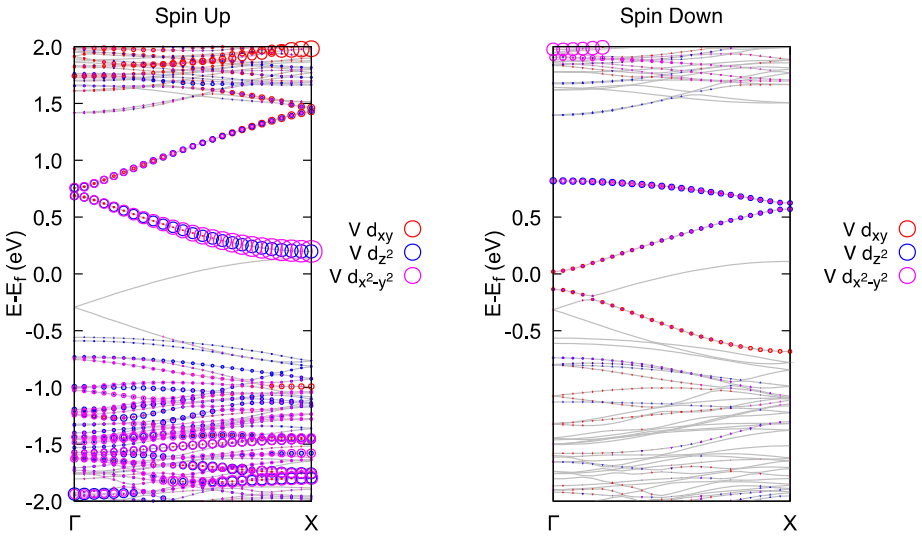

SI Figure 5. Band structures for V-alloyed S-oriented edge for 3 × periodicities when SCAN+U method is applied with U = 3eV. The symbols follow Fig. 2 in the manuscript.

---

7. Effects of SOC

In this section, the calculation details of the non-colinear calculation were illustrated and the influence of the SOC was analyzed. Generally, two-step calculations are recommended to obtain the converging non-collinear spin configurations. First, we performed collinear calculations excluding the spin-orbit coupling to obtain a relaxed structure and roughly determined the ground state of the spin configuration (ferromagnetic or anti-ferromagnetic). Then, we took the wave functions of the first step as the input to perform non-collinear calculations after including spin-orbit coupling. It often helps the code to find a true ground state rather than be trapped in the local minimum. The non-collinear calculations are often time-consuming, and it takes over 100 electronic steps to complete one ion step in our calculations. Furthermore, because of the magnetic anisotropy caused by spin-orbit coupling, different orientations of the spin axes should be carefully examined, and the easy axis should be searched. Besides, the band structure of the SOC calculations was shown here.

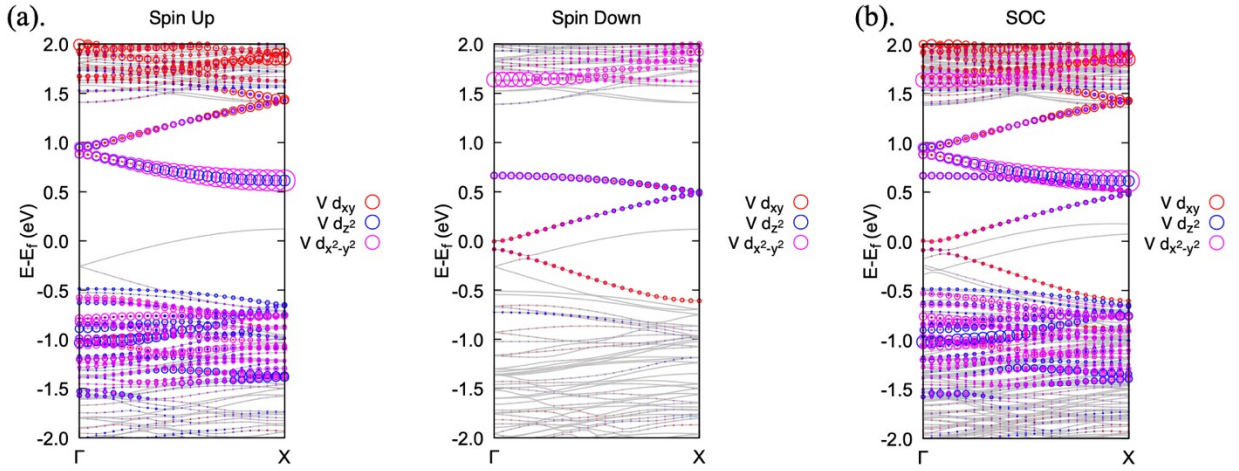

SI Figure 6. Comparison of edge states without and with SOC for the V alloyed edges with 3 × periodicities. (a) Spin-up channel without SOC; (b)spin-down channel without SOC; (c) with SOC.

8. Projected density states calculations

In this section, we have plotted the projected density states for V-alloyed S-oriented edge with 3 × periodicities, including the edge V and S atoms, and sub-edge Mo atoms, as shown in SI Fig.7. It can be observed that V d orbitals at the edge and Mo d orbitals at the sub-edge mixed and dominated the electronic behavior near the Fermi level for the spin-down channel, which is consistent with our band-structure calculations. Also, the magnetized Mo d orbitals at the sub-edge contribute more than the V d orbitals at the edge, serving as an explanation that why Mo d orbitals dominate in our Wannier calculations.

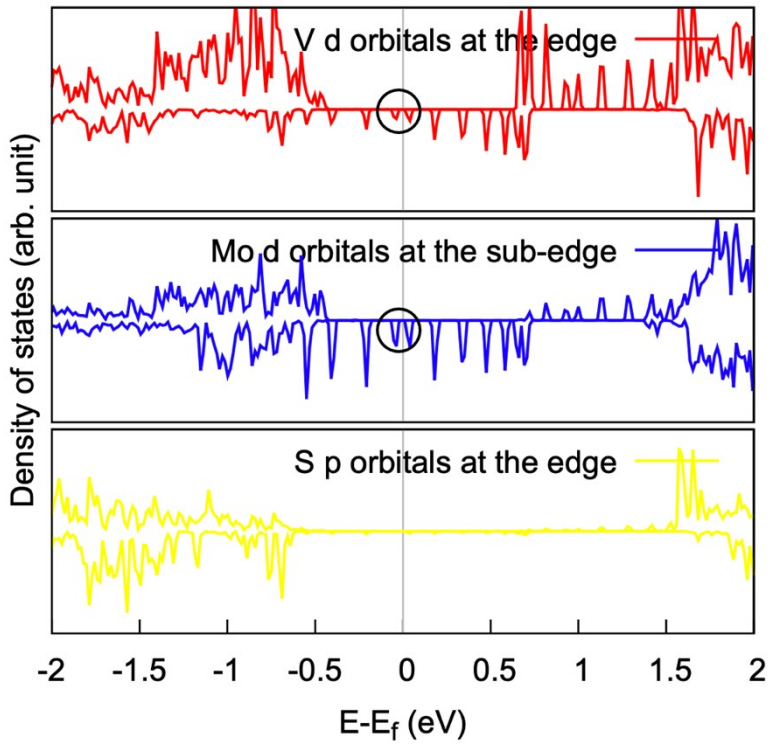

SI Figure 7. Projected density states for V-alloyed S-oriented edge with 3 × periodicities. The edge V d orbitals, edge S p orbitals, and sub-edge Mo d orbitals are represented as red, yellow, and blue colors. The picks near the Fermi level for the spin-down channel are stressed.

---

9. Method to extract the three-band model from full Hamiltonian

In this section, we illustrated the numerical projection method to obtain the effective three-band Hamiltonian from the full Hamiltonian obtained from MLWF[15]. Because the three edge bands near the Fermi level are isolated from other bulk bands, it's reasonable to assume that the three edge bands are nearly decoupled with the bulk bands and that the influence of the bulk bands can be safely neglected. We mainly focus on the eigenvalues and eigenvectors at Γ point since the gap is located at Γ point. Firstly, from MLWF, we obtained the three eigenenergies, E_1, E_2, E_3, with $E_1 < E_2 < E_3$, and the corresponding wavefunctions of the full Hamiltonian at Γ point ψ_1, ψ_2, ψ_3, near the Fermi level. Such three eigenenergies are corresponding to energies of $k = 0, \pm\frac{2}{3}\pi$ for 1 × periodicity based on band-unfolding analysis. The gap E_g is represented as $E_2 - E_1$. Next, to derive the effective Hamiltonian, we analyzed the contributions of different Wannier orbitals of the edge bands and chose the sets that contribute the most as the basis of the three-band Hamiltonian. For example, from our calculations, for the V-alloyed edge, the three Wannier functions of d_{x2-y2} shape contribute nearly 50% components of the edge bands. Therefore, we could use the three Wannier functions as the basis to project the full Hamiltonian to this much smaller Hilbert space. The projection operator is defined as:

$$\hat{P} = \sum_{i=1}^{3} |\phi_i\rangle\langle\phi_i|,$$

where ϕ_i ($i = 1\sim3$) are the Wannier functions, which are treated as the basis of the effective Hamiltonian. Then the projected wavefunction can be written as $\hat{P}\psi_1$, $\hat{P}\psi_2$, and $\hat{P}\psi_3$. If the three edge bands are totally decoupled with the other bulk bands, we could simultaneously diagonalize the full Hamiltonian and the effective Hamiltonian, therefore, the $\hat{P}\psi_1$, $\hat{P}\psi_2$, and $\hat{P}\psi_3$ can form an orthogonal basis. However, due to the coupling between the edge bands and the bulk bands, the projection orbitals are not exactly orthogonal. Still, we could use the Gram-Schmidt process to obtain the orthogonal basis $\{\hat{P}\psi_1, \hat{P}\psi_2', \hat{P}\psi_3'\}$ if the couplings between $\hat{P}\psi_1$, $\hat{P}\psi_2$, and $\hat{P}\psi_3$ are small[16]. Note, since we cared most about the wavefunctions near the Fermi level, we chose the $\{\hat{P}\psi_1, \hat{P}\psi_2, \hat{P}\psi_3\}$ as the projection order to preserve the wavefunction of $\hat{P}\psi_1$. Finally, we could obtain the effective Hamiltonian via:

$\hat{H}_{eff} = \left(\hat{P}\psi_1, \hat{P}\psi_2', \hat{P}\psi_3'\right) diag(E_1, E_2, E_3) \left(\hat{P}\psi_1, \hat{P}\psi_2', \hat{P}\psi_3'\right)^{\dagger}$.

10. Wannier functions of intrinsic S-oriented edge

In this section, we investigated the Wannier function sets to describe the three edge bands for the intrinsic S-oriented edge. As shown in SI Fig.8(a)-(f), the major contributions of the edge bands are from d_{x2-y2} and d_{z2} orbitals mainly located at the edge Mo atoms at the S-oriented edge. The Wannier function analysis is also consistent with the edge Mo components obtained from DFT calculations, as shown in SI Fig.8(g). Because the contributions of the $\{d_{x2-y2}\}$ and $\{d_{z2}\}$ sets are close and they are mixed to form the three-edge bands in the gap, we performed the projections for $\{d_{x2-y2}\}$ and $\{d_{z2}\}$ sets and obtain the Hamiltonian based on each set separately. We then listed the onsite energy and hopping integrals based on the two sets in SI Table 1 with $u < v < w$ applied. We noted that the hopping integrals of two sets are different and the $\{d_{z2}\}$ set is more localized with smaller hopping integrals. The band-structure based on the $\{d_{x2-y2}\}$ and $\{d_{z2}\}$ dominated Wannier functions are also shown in the SI Fig.8(h) and (I), respectively. Because of the mixture of the two sets and the influence of the bands from the bulk, neither of them could fully reproduce the dispersion relationship of the edge bands obtained from the DFT calculations. Still, it may indicate that the nearly flat edge bands are mainly from the large inequivalence of the hopping integrals between nearby $\{d_{z2}\}$ orbitals, as shown in Fig. 8(I). Note we mainly focus on the $\{d_{x2-y2}\}$ dominated Wannier functions in the manuscript.

SI Table 1: Parameters of trimer SSH model according to the projection of the subspace spanned by three edge bands based on $\{d_{x2-y2}\}$ and $\{d_{z2}\}$ dominated sets for the intrinsic edge at the Γ point, respectively. Here we have chosen the parameters to satisfy $w > u,v$.

Parameters	μ_A	μ_B	μ_C	u	v	w
$\{d_{x2-y2}\}$	-2.93 eV	-3.19 eV	-2.73 eV	0.12 eV	-0.28 eV	0.35 eV
$\{d_{z2}\}$	-2.62 eV	-3.33 eV	-2.89 eV	0.02 eV	-0.25 eV	0.28 eV

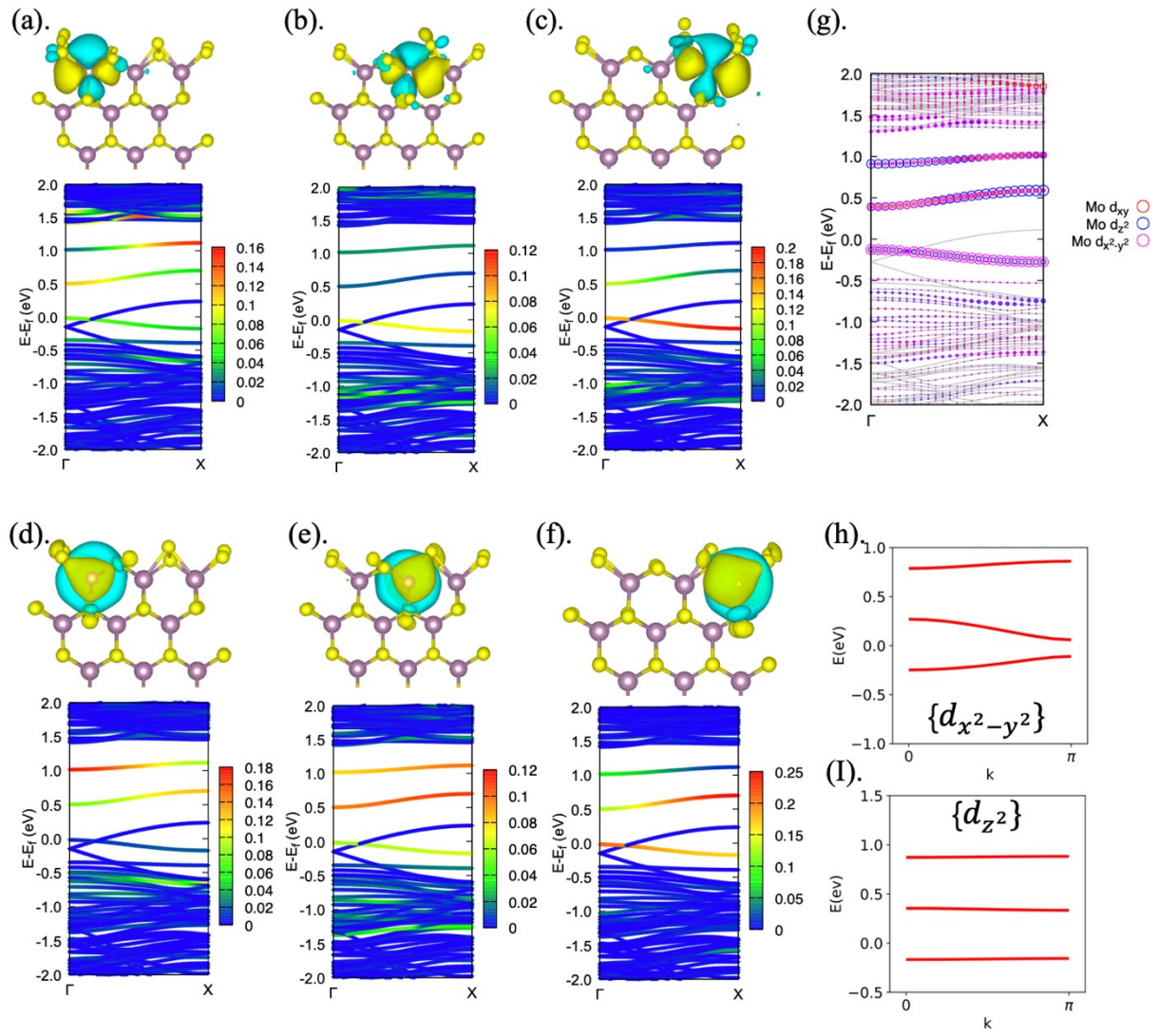

SI Figure 8. (a), (b), (c): Wannier representations and visualization of the $\{d_{x2-y2}\}$ set. (d), (e), (f):Wannier representations and visualizations of the $\{d_{z2}\}$ set for the edge state of the intrinsic edge with 3 × periodicities. The symbols follow Figure 4 in the manuscript. (g): Edge Mo component for the edge bands from DFT calculations. (h).(I): Three-band tight-binding models based on Wannier function sets $\{d_{x2-y2}\}$ and $\{d_{z2}\}$, respectively.

11. Wannier functions of the spin-up channel of V-alloyed edge

In this section, we investigated the Wannier functions of the spin-up channel of the V-alloyed edge, which is located above the Fermi energy. The contributions of the spin-up channel are from d_{x2-y2} orbitals mainly located at three V atoms at the edge, as shown in SI Fig.9(a)~(c), which is different from the spin-down channel as illustrated in the manuscript. The Wannier function analysis is also consistent with the edge V components obtained from DFT calculations, as shown in SI Fig.9(d). Note, since the top edge band is largely mixed with the conduction bands, it's difficult to obtain the accurate value of the hopping integrals from the three-band model. However, we can still find a gap opening of about 69meV near the 1eV above the Fermi level. Such gap opening can also be a signature of the edge reconstruction, similar to the spin-down channel.

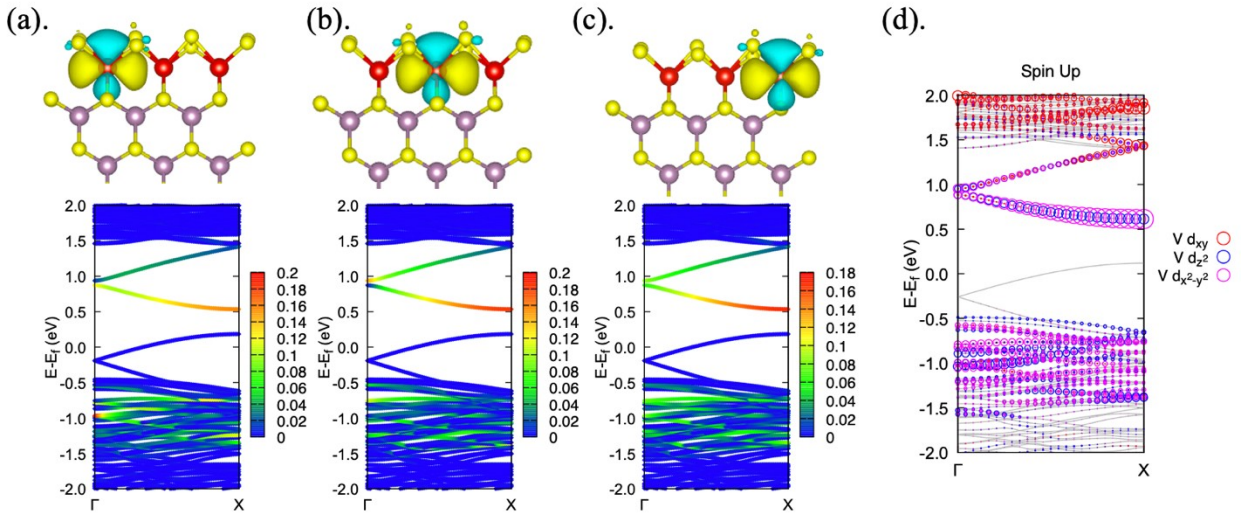

SI Figure 9. (a), (b), (c): Wannier representations and visualizations for the edge states of the V alloyed edge with 3 × periodicities in the spin-up channel. The symbols follow Figure 4 in the manuscript. (d): Edge V component for the edge bands from DFT calculations.

Reference:

(1) Mermin, N. D.; Wagner, H. Absence of Ferromagnetism or Antiferromagnetism in One-or Two-Dimensional Isotropic Heisenberg Models. *Phys. Rev. Lett.* **1966**, *17* (22), 1133.

(2) Wang, M.-C.; Huang, C.-C.; Cheung, C.-H.; Chen, C.-Y.; Tan, S. G.; Huang, T.-W.; Zhao, Y.; Zhao, Y.; Wu, G.; Feng, Y.-P.; others. Prospects and Opportunities of 2D van Der Waals Magnetic Systems. *Ann. Phys.* **2020**, *532* (5), 1900452.

(3) Martinez Alvarez, V. M.; Coutinho-Filho, M. D. Edge States in Trimer Lattices. *Phys. Rev. A* **2019**, *99* (1), 13833. https://doi.org/10.1103/PhysRevA.99.013833.

(4) Bao, K.; Zhu, J. A Brief Review of Reconstructions and Electronic Structures of MoS2 Zigzag Edges. *J. Appl. Phys.* **2022**, *132* (8), 80702.

(5) Lucking, M. C.; Bang, J.; Terrones, H.; Sun, Y. Y.; Zhang, S. Multivalency-Induced Band Gap Opening at MoS2 Edges. *Chem. Mater.* **2015**, *27* (9), 3326–3331. https://doi.org/10.1021/acs.chemmater.5b00398.

(6) Sin, C.-K.; Zhu, J. Determining Equilibrium Shapes of MoS2: Modified Algorithm, Edge Reconstructions with S and O, and Temperature Effects. *J. Phys. Chem. C* **2021**, *125* (8), 4828–4835.

(7) Zhang, J.; Zhao, W.; Zhu, J. Missing Links towards Understanding the Equilibrium Shapes of Hexagonal Boron Nitride: Algorithm, Hydrogen Passivation, and Temperature Effects. *Nanoscale* **2018**, *10* (37), 17683–17690.

(8) Himmetoglu, B.; Floris, A.; De Gironcoli, S.; Cococcioni, M. Hubbard-Corrected DFT Energy Functionals: The LDA+ U Description of Correlated Systems. *Int. J. Quantum Chem.* **2014**, *114* (1), 14–49.

(9) Cococcioni, M. The LDA+ U Approach: A Simple Hubbard Correction for Correlated Ground States. *Correl. Electrons From Model. to Mater. Model. Simul.* **2012**, *2*.

(10) Bruus, H.; Flensberg, K. Introduction to Many-Body Quantum Theory in Condensed Matter Physics. *Univ. Copenhagen* **2002**.

(11) Long, O. Y.; Gautam, G. S.; Carter, E. A. Evaluating Optimal U for 3 d Transition-Metal Oxides within the SCAN+ U Framework. *Phys. Rev. Mater.* **2020**, *4* (4), 45401.

(12) Zhou, J.; Zhang, W.; Lin, Y.-C.; Cao, J.; Zhou, Y.; Jiang, W.; Du, H.; Tang, B.; Shi, J.; Jiang, B.; others. Heterodimensional Superlattice with In-Plane Anomalous Hall Effect. *Nature* **2022**, *609* (7925), 46–51.

(13) Tolba, S. A.; Gameel, K. M.; Ali, B. A.; Almossalami, H. A.; Allam, N. K. The DFT+ U: Approaches, Accuracy, and Applications. *Density Funct. Calc. Progresses Theory Appl.* **2018**, *1*, 5772.

(14) Sun, J.; Ruzsinszky, A.; Perdew, J. Strongly Constrained and Appropriately Normed Semilocal Density Functional. *Phys. Rev. Lett.* **2015**, *115* (3), 1–6. https://doi.org/10.1103/PhysRevLett.115.036402.

(15) Pizzi, G.; Vitale, V.; Arita, R.; Blügel, S.; Freimuth, F.; Géranton, G.; Gibertini, M.; Gresch, D.; Johnson, C.; Koretsune, T.; others. Wannier90 as a Community Code: New Features and Applications. *J. Phys. Condens. Matter* **2020**, *32* (16), 165902.

(16) Cheney, W.; Kincaid, D. Linear Algebra: Theory and Applications Sudbury. *Ma Jones Bartlett* **2009**.